Rapid onset of mafic magmatism facilitated by volcanic edifice collapse

M. Cassidy, S F L Watt, P. J. Talling, M. R Palmer, M. Edmonds, M. Jutzeler, D. Wall-Palmer, M. Manga, M. Coussens, T. Gernon, et al.

AGU PUBLICATIONS

Geophysical Research Letters

RESEARCH LETTER
10.1002/2015GL064519

Key Points:
- Marine cores record eruption deposits overlying a 6–10 km^3 collapse deposit
- A shift from andesitic to basaltic compositions follows flank collapse
- Pre-P-T and post-P-T ascent paths show rapid ascent from the midcrust

Supporting Information:
- Text S1, Figures S1–S4, and Tables S1–S4

Correspondence to:
M. Cassidy,
mcassidy@uni-mainz.de

Citation:
Cassidy, M., et al. (2015), Rapid onset of mafic magmatism facilitated by volcanic edifice collapse, *Geophys. Res. Lett.*, *42*, 4778–4785, doi:10.1002/2015GL064519.

Received 11 MAY 2015
Accepted 20 MAY 2015
Accepted article online 25 MAY 2015
Published online 17 JUN 2015

Rapid onset of mafic magmatism facilitated by volcanic edifice collapse

M. Cassidy[1,2], S. F. L. Watt[1,3], P. J. Talling[4], M. R. Palmer[1], M. Edmonds[5], M. Jutzeler[4], D. Wall-Palmer[6], M. Manga[7], M. Coussens[4], T. Gernon[1], R. N. Taylor[1], A. Michalik[1], E. Inglis[1], C. Breitkreuz[8], A. Le Friant[9], O. Ishizuka[10], G. Boudon[9], M. C. McCanta[11], T. Adachi[12], M. J. Hornbach[13], S. L. Colas[9], D. Endo[14], A. Fujinawa[15], K. S. Kataoka[16], F. Maeno[17], Y. Tamura[18], and F. Wang[19]

[1]Ocean and Earth Science, University of Southampton, Southampton, UK, [2]Institute for Geosciences, Johannes Gutenberg University, Mainz, Germany, [3]School of Geography, Earth and Environmental Sciences, University of Birmingham, Birmingham, UK, [4]Marine Geosciences, National Oceanography Centre, Southampton, UK, [5]Department of Earth Sciences, University of Cambridge, Cambridge, UK, [6]School of Geography, Earth and Environmental Sciences, Plymouth University, Plymouth, UK, [7]Department of Earth and Planetary Science, University of California, Berkeley, California, USA, [8]Institut für Geologie und Paläontologie, Technische Universität Bergakademie, Freiberg, Germany, [9]Équipe de Géologie des Systèmes Volcaniques, Institut de Physique du Globe de Paris, Sorbonne Paris Cité, UMR 7154 CNRS, Paris, France, [10]Geological Survey of Japan (AIST), Tsukuba, Japan, [11]Department of Geology, Tufts University, Medford, Massachusetts, USA, [12]Department of Earth and Environmental Science, Yamagata University, Yamagata, Japan, [13]Institute for Geophysics, University of Texas, Austin, Texas, USA, [14]Earth Evolution Sciences, University of Tsukuba, Tsukuba, Japan, [15]Department of Earth Sciences, Ibaraki University, Mito, Japan, [16]Natural Hazards and Disaster Recovery, Niigata University, Nishi-ku, Japan, [17]Earthquake Research Institute, University of Tokyo, Bunkyo-ku, Japan, [18]Institute for Frontier Research on Earth Evolution, Japan Agency for Marine-Earth Science and Technology, Yokosuka, Japan, [19]Institute of Geology and Geophysics, Chinese Academy of Sciences, Beijing, China

Abstract Volcanic edifice collapses generate some of Earth's largest landslides. How such unloading affects the magma storage systems is important for both hazard assessment and for determining long-term controls on volcano growth and decay. Here we present a detailed stratigraphic and petrological analyses of volcanic landslide and eruption deposits offshore Montserrat, in a subduction zone setting, sampled during Integrated Ocean Drilling Program Expedition 340. A large (6–10 km^3) collapse of the Soufrière Hills Volcano at ~130 ka was followed by explosive basaltic volcanism and the formation of a new basaltic volcanic center, the South Soufrière Hills, estimated to have initiated <100 years after collapse. This basaltic volcanism was a sharp departure from the andesitic volcanism that characterized Soufrière Hills' activity before the collapse. Mineral-melt thermobarometry demonstrates that the basaltic magma's transit through the crust was rapid and from midcrustal depths. We suggest that this rapid ascent was promoted by unloading following collapse.

1. Introduction

Volcanic edifices are inherently unstable, and major collapses are an important stage in the life cycle of many volcanoes. Stratigraphic reconstructions of eruption records at several volcanoes indicate that large collapses may mark a shift in volcanic activity, with subsequent volcanism characterized by high eruptive output or a switch to more mafic magma compositions, especially at large ocean-island volcanoes [*Boudon et al.*, 2013; *Hora et al.*, 2009; *Manconi et al.*, 2009; *Presley et al.*, 1997]. These modifications in magmatic-volcanic behavior are attributed to the static decompression of stored magma bodies in response to a reduction in the load of the volcanic edifice [*Manconi et al.*, 2009; *Pinel and Jaupart*, 2005]. Testing this model is hampered by a lack of understanding of how different parts of a magma plumbing and storage system are affected by collapse. This is particularly true for arc volcanic systems, which are frequently subject to edifice collapse and which account for the majority of Earth's subaerial volcanism, but where detailed stratigraphic records of past volcanic activity are difficult to construct because of erosion and burial of eruption products. By reconstructing the history of volcanic activity before and after collapse at a well-studied arc volcano, where marine sediment cores provide an unusually detailed history of activity during the last 100 kyr, we seek to understand how collapse(s) affected the ascent of magma from depth and how this is manifested in the style and composition of subsequent volcanism. Here we provide the first attempt

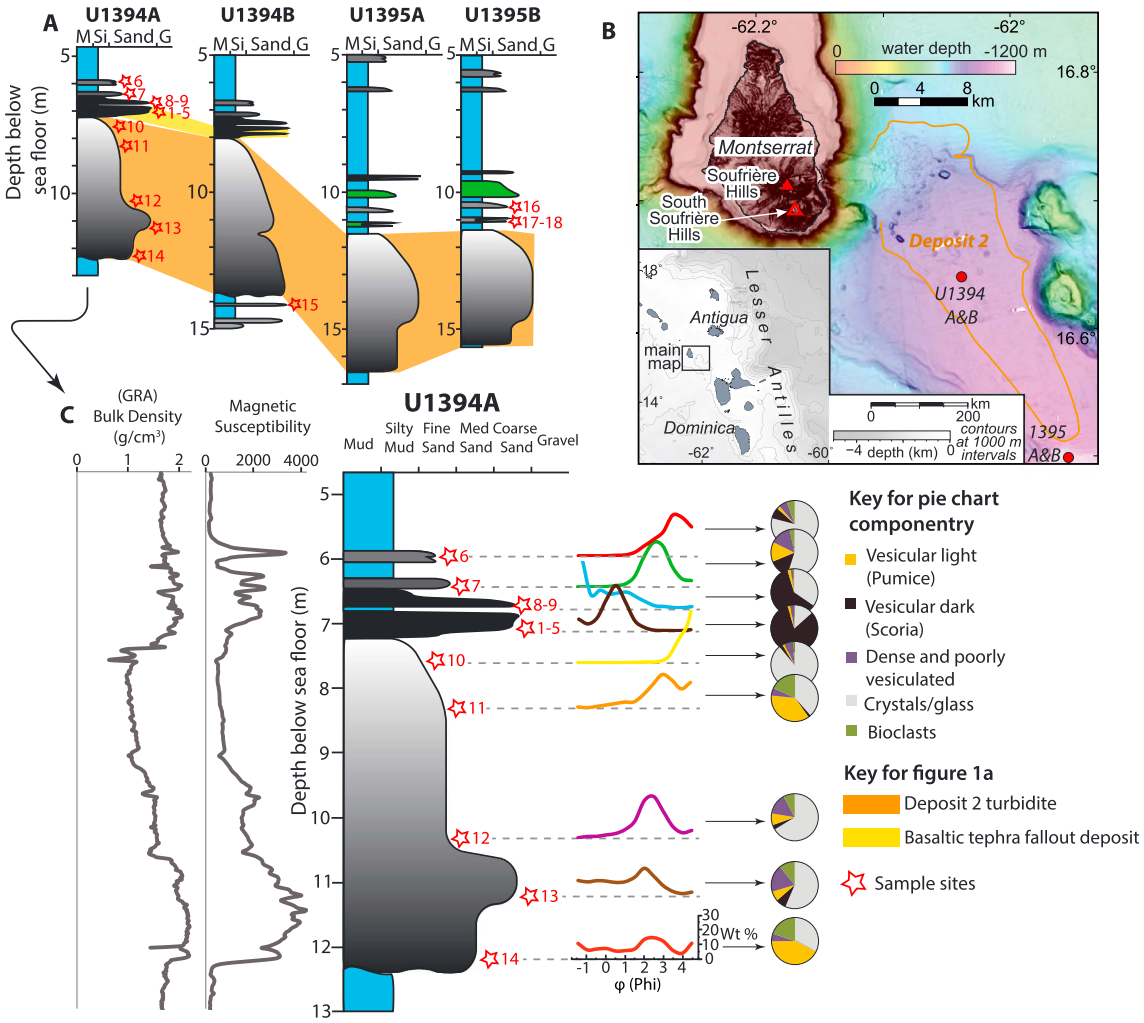

Figure 1. (a) Correlation of IODP core sections for the different deposits. Yellow is the basaltic fallout deposit, and the orange is the turbidite associated with landslide Deposit 2. M = mud, Si = silt, and G = gravel. (b) Map insert shows the location of the IODP core and debris avalanche (Deposit 2). (c) Expanded log of IODP core 1394A, with bulk density calculated by gamma ray attenuation, magnetic susceptibility, grain size histograms, and componentry pie charts.

to create *P-T* ascent paths for magmatism before and after a major landslide, thus providing new insights into how edifice collapse affects crustal magmatic processes.

1.1. Background

Montserrat is a small island in the Lesser Antilles arc with a history of moderate-scale ($<10\,km^3$) subaerial and submarine landslides [*Le Friant et al.*, 2004]. The largest landslide to affect the Soufrière Hills Volcano (SHV), the currently active center on Montserrat, is termed Deposit 2 [*Le Friant et al.*, 2004] and deposited 6–10 km^3 of material offshore [*Watt et al.*, 2012]. The SHV has consistently erupted andesitic magmas during its ~300 kyr history. A brief episode of basaltic activity at ~128–131 ka interrupted this pattern and led to construction of the adjacent mafic South Soufrière Hills (SSH) volcano [*Cassidy et al.*, 2014a; *Harford et al.*, 2002] (Figure 1).

Montserrat is an excellent case study for a coupled petrological and stratigraphic investigation of volcanic activity before and after a major collapse, because the onshore, offshore, and subsurface geology are well constrained by petrological and geophysical studies [*Druitt and Kokelaar*, 2002; *Sevilla et al.*, 2010; *Wadge et al.*, 2014]. We make use of an Integrated Ocean Drilling Program (IODP) Expedition 340 core data set, which recovered meter-thick volcaniclastic deposits (mass flow and fallout deposits), previously unreachable by shallow coring, to investigate volcanic activity in the period before and after the Deposit 2 collapse.

2. Methods and Materials

IODP Expedition 340 collected sediment cores to depths of up to 200 m from four sites around Montserrat [*Le Friant et al.*, 2015]. The samples studied here come from Sites U1394 and U1395, SE of Montserrat (Figure 1). The cores were visually logged and sampled for measurements of grain size and componentry using the methods of *Cassidy et al.* [2014a, 2014b]. Unaltered grains were picked for major, trace element and Pb isotopic analysis using XRF, inductively coupled plasma–mass spectrometry (ICP-MS), and multiple collection ICP-MS instruments, respectively, as described by *Cassidy et al.* [2012]. Thin sections of clasts containing clinopyroxene phenocrysts and other primary mineral phases were analyzed by electron microprobe (see supporting information for full methods).

2.1. Chronology and Characteristics of Deposits

Cores from Sites U1394 and U1395 (Figure 1) each preserve sequences of bioclastic and volcaniclastic deposits, separated by, hemipelagic intervals, providing a record of mass flows and fall deposits originating from Montserrat. The volcanic material within these deposits comprises common fragmented crystals, scoria, poorly vesiculated lava fragments, and some pumice-rich lenses; selected grains of which were picked for geochemical and petrological analyses. The top of an unusually thick (~7 m) turbidite occurs in U1394 and U1395 at 7 and 12 m below seafloor, respectively (it is easily correlated between Sites U1394 and U1395 due to its anomalous thickness and composition (Figure 1 and Figure S1 in the supporting information)). This distinctive turbidite contains a mixture of coarse (up to coarse sand) and poorly sorted volcanic, bioclastic, and terrigenous clasts (Figure 1). The lack of sharp stratigraphic boundaries and presence of grading within the visual and multisensor core logging of the turbidite suggest that it was not a result of postdrilling disturbance but emplaced as one large progressively aggrading current. The depth below seafloor, distribution, and thickness of this turbidite are consistent with it being generated by the Deposit 2 landslide, which has been mapped offshore by geophysical surveys [*Le Friant et al.*, 2004; *Watt et al.*, 2012] (Figure 1b).

Directly overlying Deposit 2 (with no visible intervening hemipelagic sediment) is a distinctive layer, rich in basaltic scoria. This scoria-rich layer likely records an explosive basaltic eruption, because it is much better sorted than the underlying Deposit 2 turbidite, has a consistent and homogenous composition (60–82% basaltic scoria; Figure 1c) with very few bioclasts compared to adjacent turbidites, and the vesicularity of the angular basaltic clasts ranges from 20% to 46%, suggesting material formed in an explosive event. Given this interpretation, this fallout layer should not have an erosive basal surface. Thus, the lack of any visible hemipelagic sediment between the basaltic layers and the Deposit 2 turbidite suggests that the onset of basaltic volcanism following the Deposit 2 landslide was rapid. We estimate a time period of $<$100 years, and potentially much less, given that the local hemipelagic sedimentation rate of 0.05 m ka^{-1} [*Trofimovs et al.*, 2010] suggests that 5 mm of sediment would have accumulated in this period, and we would expect this to be visible.

An ~20 cm thick hemipelagic mud interval overlies the basaltic fallout layer (indicating a time period of ~4 ka based on local sedimentation rates). The base of this hemipelagic layer can be dated using an oxygen isotope stratigraphic record (Site U1395B) to $>$123 ka, because it contains the peak negative excursion during marine isotope stage 5.5 (Figure S1 in the supporting information). This indicates that Deposit 2 and the overlying basaltic deposits are slightly older than 123 ka.

Based on close similarities in major and trace element and isotope compositions (Table S1 in the supporting information), this basaltic fallout deposit likely derives from the SSH. Ar-Ar dates of SSH volcanism cluster at ~128–131 ka [*Harford et al.*, 2002], providing a strong temporal basis for the correlation of SSH with the basaltic deposits overlying the Deposit 2 turbidite and further constraining the age of Deposit 2 to ~130 ka.

The rarity of basaltic material in volcaniclastic horizons below the Deposit 2 turbidite suggests that the basaltic deposit immediately above the turbidite represents the earliest stages of eruption from SSH and that the SSH eruptions followed Deposit 2, rather than the reverse. Samples from this basaltic deposit (1–5) also indicate that it is more primitive than younger basaltic deposits in the cores (Table S1 in the supporting information). The mineral assemblage comprises plagioclase, clinopyroxene, orthopyroxene, olivine, and oxides (Figure S2 in the supporting information). The pyroxenes used for this study lacked any disequilibrium textures such as zoning, growth banding, cellular or sieve textures, resorption, or

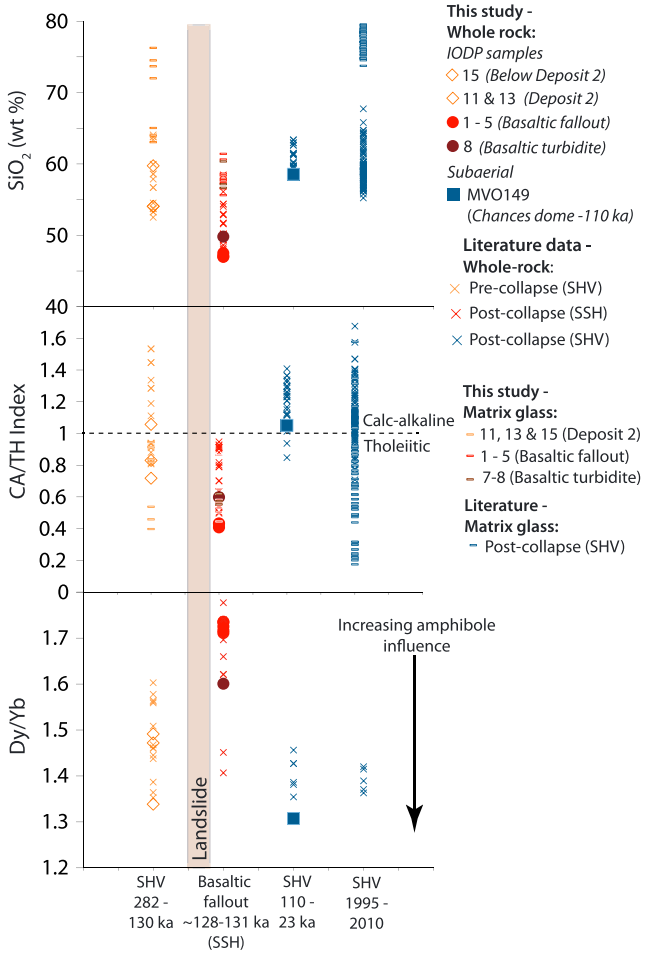

Figure 2. Chemical changes through prelandslide and postlandslide transition. Volcanism that occurred at 282 to 174 ka was not at the SHV site but is thought to represent the same system and thus grouped here. Sample numbers refer to the sites shown in Figure 1. Literature data from *Horwell et al.* [2001], *Zellmer et al.* [2003], and *Cassidy et al.* [2012]. Matrix glass data for this study can be found in Table S2 in the supporting information. Matrix glass data for the SHV 1995–2010 from *Humphreys et al.* [2010].

reaction rims (Figure S2 in the supporting information). In addition, the similarity of core and rim analyses indicates that most crystals are unzoned and homogenous.

Additional basaltic deposits occur at both core sites above the ~4 ka hemipelagic interval. In contrast to the deepest basaltic fallout layer, these younger deposits are poorly sorted, containing a more diverse componentry (including andesitic clasts) and show polymodal grain size distributions [*Cassidy et al.*, 2014a, 2014b]. Thus, these later deposits likely represent the emplacement of turbidity currents containing reworked volcanic material, originating from the erosion of eruption deposits from the SSH (samples 7 and 8).

2.2. Chemical and Mineralogical Transitions Following Collapse

The whole-rock and matrix glass chemistry of volcaniclastic components in the IODP 340 core stratigraphy indicate that distinct magmatic changes took place at ~130 ka on Montserrat (Figure 2). Specifically, a sharp transition to basaltic compositions appears immediately above the Deposit 2 turbidite in the IODP cores and correlates with terrestrial samples from the SSH, with both events independently dated at ~130 ka. The basaltic fallout layer represents a period of explosive volcanism, before activity on Montserrat returned to intermediate silicic magmas from 110 ka to present (Figure 2). Changes in Fe and Mg bulk rock concentrations are also reflected in the calc-alkaline/tholeiitic index [*Hora et al.*, 2009], which shows that SSH magmas became more tholeiitic immediately after the ~130 ka collapse, with calc-alkaline compositions returning to the SHV at ~110 ka. The high values of Dy/Yb in the SSH samples relative to SHV are also indicative of less amphibole crystallization at the SSH [*Davidson et al.*, 2007] and accord with the apparent absence of amphibole within the SSH assemblages (Figure 2).

2.2.1. Mineralogical Changes Within the SHV

The SHV products that erupted before and after Deposit 2 show changes in the mineral phase assemblage, which may indicate a postcollapse effect on the andesitic magma storage system. Although amphibole is occasionally present in pre-Deposit 2 volcanics, it is rare and often heavily altered; in general, two pyroxene andesites dominate [*Harford et al.*, 2002]. In contrast, amphibole becomes a major phenocryst phase within SHV magmas younger than 110 ka, and clinopyroxene is rare and occurs only as patchy overgrowths on orthopyroxenes and amphiboles. Despite this mineralogical transition, the Dy/Yb ratios are only very slightly lower in the younger SHV rocks (Figure 2). This suggests that amphibole crystallization was likely cryptic (absent in the assemblage) within the prelandslide SHV magmas but stable over a broader pressure range in the postlandslide SHV magmas. The reasons for this mineralogical change

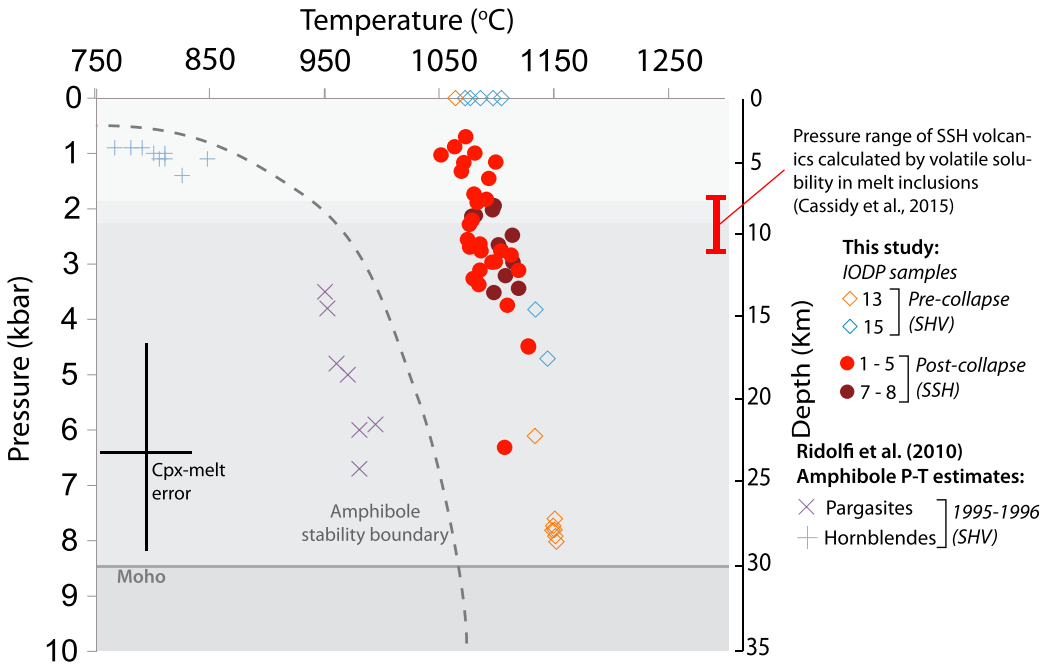

Figure 3. *P-T* paths from clinopyroxene-liquid pairs and amphibole thermobarometry data from *Ridolfi et al.* [2010]. Each pyroxene core represents an average of at least four probe analyses (Table S3 in the supporting information). The grey dashed line represents the amphibole stability boundary from *Ridolfi et al.* [2010]. Depths are based on crustal structural studies of Montserrat [*Sevilla et al.*, 2010], and the background shading is based on crustal discontinuities, with darker shading indicating faster *P* wave velocities. Sample numbers refer to the sites shown in Figure 1.

remain unclear but may indicate slight thermal or compositional shifts in the nature of the upper crustal magma storage system after collapse.

2.3. Magma Ascent Paths

While magmatic storage/transport depths are often estimated from volatile (CO_2 and H_2O) saturation pressures measured by secondary ion mass spectrometry on melt inclusions, CO_2, H_2O, and other volatiles partially degas before crystallization takes place [*Blundy et al.*, 2010]. Hence, melt inclusions generally only record shallower pressures within the upper crust (3–4 kbar [*Metrich and Wallace*, 2008]), where they are formed under a specific set of conditions (i.e., fast cooling). To investigate deeper crustal processes, we have used clinopyroxene phenocryst core-liquid pairs to reconstruct *P-T* paths (Figure 3), because this method is able to provide estimates of conditions during early stages of crystallization [*Armienti et al.*, 2013; *Putirka and Condit*, 2003; *Putirka et al.*, 2003] (Table S3 in the supporting information). Uncertainties in clinopyroxene crystallization pressures estimated by this method are ~2 kbar.

Although the SSH magmas show evidence of hybridization between melts and crystal mushes [*Cassidy et al.*, 2015], the basaltic fallout samples examined here (thought to be the earliest SSH magmas) show limited evidence for mixing and are therefore the best means of estimating liquid compositions remains the use of whole-rock data, in the absence of other information. To verify that the clinopyroxene cores were in equilibrium with the whole-rock compositions (which are used to derive estimates of liquid compositions) and to strengthen the validity of our approach, the following approach was applied: (a) visibly zoned crystals were avoided (Figure S2 in the supporting information); (b) minor amounts of olivine and pyroxene were subtracted (<10%) from the whole-rock compositions along a liquid line of descent to ensure that clinopyroxene and whole-rock pairs were in equilibrium, using the Fe-Mg exchange $K_D^{cpx\text{-}liq}(\text{Fe-Mg}) = 0.27 \pm 0.03$ [*Putirka et al.*, 2003]; (c) a comparison was made between cpx-liquid and olivine-liquid thermometry, showing a close correlation of melt temperatures (Figure S3 in the supporting information); and (d) the predicted versus observed clinopyroxene compositional components were calculated and show close correlations with sums that approach unity (Figure S4 in the supporting

information), suggesting that all phases are adequately accounted for in our method. Any points, which lay outside the 2 sigma error for predicted clinopyroxene components, were eliminated (7 out of 65 points).

The clinopyroxene thermobarometric results (Figure 3) show that the prelandslide volcanic products from SHV (samples 13 and 15) are partly clustered in *P-T* space, particularly sample 13 at ~8 kbar, with sample 15 indicating crystallization depths of ~4–5 kbar (corresponding to depths of ~28 and 16 km, respectively, for a lithostatic pressure gradient of 0.29 kbar/km). The growth of clinopyroxene at near-surface pressures likely represents the conversion of amphiboles, unstable at low pressures, during final ascent and eruption [*Smith*, 2014].

The earliest basaltic magmas (immediately postlandslide; samples 1–5) form an array in *P-T* space that is indicative of continuous crystallization across a pressure interval of ~1 to 5 kbar (~3–17 km, assuming that magmastatic pressures are equal to lithostatic pressures; if an exsolved, coupled gas phase exists then elevated magmastatic pressures would reduce this depth range, but the major result of a subvertical *P-T* array spanning the midcrustal region still holds). The wide pressure distribution of the SSH data (which exceeds the margins of error) compared to the clusters of the SHV magmas within *P-T* fields suggests that crystallization of the SSH magmas occurred during ascent through the crust rather than at specific depths. This supports the notion that the SSH magmas did not stagnate in the crust and either crystallized during ascent or tapped multiple small bodies across a range of crustal depths. The fact that the SSH data lie on a subvertical line indicates that minimal heat was lost for a large given pressure decrease, suggesting rapid ascent of the magma and supporting our stratigraphic inference of a short period between the Deposit 2 collapse and the eruption of the SSH basaltic magmas. Coupled with petrological interpretations of hybridization in the SSH magmas [*Cassidy et al*., 2015], our results are consistent with the rapid ascent of a magma that assembled material from melt lenses across a range of crustal depths prior to eruption.

In contrast to the SHV magmas, there is no evidence that clinopyroxene in the SSH magmas underwent retrograde reaction, most likely because they maintained sufficiently high temperatures and rapid ascent paths to avoid crossing the amphibole stability boundary (Figure 3). Thus, the SSH magmas preserve the record of crystallization pressures and temperatures upon ascent (Figure 3). A comparison with the currently active SHV system comes from amphibole thermobarometry [*Ridolfi et al*., 2010], because the postcollapse SHV lacks clinopyroxene. Although care should be taken when comparing these two different thermobarometers, the pargasite-hornblende data show two *P-T* regions: a deeper region associated with pargasites in mafic enclaves, and reflecting a midcrustal mafic magma source region, and a clustered shallow region, representing the upper crustal andesitic SHV magma reservoir. However, a recent study suggests that these calculated crystallization pressures should be treated with some caution and that the range of pressures derived from amphibole barometry may simply reflect compositional variations rather than separate storage regions [*Erdmann et al*., 2014]. Despite this, both regions lie at lower temperatures relative to the cpx-thermometry for the SSH volcanic system, within the amphibole stability field (Figure 3).

2.3.1. Rapid Ascent of Mafic Magma From Midcrustal Depths

Mafic magmas are less commonly erupted at subduction zones than more felsic magmas due to their greater bulk density relative to the crust; nevertheless, several factors may contribute to the rapid ascent and eruption of deeper, mafic magma in this instance. A decompression event, such as unloading from a landslide, extensional faulting, or glacial melting may reduce the rupture pressure of a stored magma body at depth, thus promoting dike formation [*Gee et al*., 1998; *Manconi et al*., 2009; *Pinel and Jaupart*, 2005]. This rapid ascent at relatively high temperatures ensures that crystals such as amphibole are not formed in the midcrust, which would otherwise decrease the ascent rate by stalling the magma and removing volatiles (Figure 3). The lack of amphibole crystallization also likely contributes to the tholeiitic nature of the SSH magmas, which would otherwise act to enrich the residual melt in SiO_2 and TiO_2, thus driving calc-alkaline fractionation [*Davidson et al*., 2007]. The deep melts that are mobilized by the edifice collapse do not necessarily lie in a single storage region; rather, they may represent multiple bodies that have incorporated crystals on their ascent to give the hybridized lava observed at the surface [*Cassidy et al*., 2015].

Postcollapse volcanism commonly occurs at the site of the unloading; however, in this instance, the site of SSH volcanism is concentrated to the south of the SHV (Figure 1). One explanation for this is that the higher density magmas could be making use of a regional fault network which is present around

Montserrat [*Cassidy et al*., 2012]. Or potentially, the denser magmas may be deflected by an overlying load [*Pinel and Jaupart*, 2000]. Often intermediate to rhyolitic magma reservoirs can obstruct the passage of mafic magma, explaining why basaltic eruptions often only reach the surface on the periphery of silicic volcanoes [*Hildreth*, 1981].

It is difficult to quantify precisely the impact of surface unloading by edifice collapse on subsurface magma systems, given an absence of data on system geometry. Here we suggest that magmas rise from midcrustal levels following collapse, and we can estimate the pressure change induced by collapse at this depth, following the method in *Pinel and Albino* [2013]. Deposit 2 has a volume of 10 km^3, including a poorly constrained proportion of marine sediment [*Watt et al*., 2012]. For a volcanic collapse volume of 6 km^3, assuming a conical collapse geometry and a slope gradient of 14°, a vertical mass of ~700 m is removed above the vent. At 10 km depth, this produces a vertical stress reduction of 0.6 MPa and a pressure reduction of 0.18 MPa (calculations assume an elastic, homogeneous medium, using a density of 2500 kg m^{-3} and a Poisson's ratio of 0.25 [cf. *Pinel and Albino*, 2013]). Although there are uncertainties in the above parameters, this will not affect the order of magnitude of the pressure change, and the calculation is illustrative of the effect that surface unloading may have in the midcrust. Magma storage systems may reside in a delicate balance, and a change of this magnitude may enable magma overpressure in storage regions to exceed lithostatic forces and initiate dike formation. Our calculated pressure drop is comparable to the ~0.5 MPa calculated to have affected the magma source region at El Hierro following the El Golfo flank collapse [*Manconi et al*., 2009], and it far exceeds the dynamic stress changes affecting magma storage systems following large, distal earthquakes ($<10^{-2}$ MPa), which have been postulated as an eruption trigger in several cases [*Manga and Brodsky*, 2006]. A pressure drop on this order compares to critical overpressures for dike formation of up to a few megapascal for basaltic systems [*Gudmundsson*, 2012], and a pressure drop on the order of 10^{-1} MPa could therefore plausibly perturb the system. However, the relationship between pressure reduction from surface unloading and the ultimate impact on the magma system is not simple. *Pinel and Albino* [2013] note that pressure reductions in some scenarios may reduce eruption likelihood, with the magmatic response not only dependent on total pressure decrease but also on the storage depth and geometry of the system.

In summary, although there is previous evidence from several locations that mafic volcanism may follow unloading of the magmatic plumbing system by large flank collapses [*Hora et al*., 2009; *Manconi et al*., 2009], this contribution is the first to place constraints on the source region of these magmas and to show that the transition to mafic magmatism can be rapid (on time scales of <100 years). We hypothesize here that these mafic volcanic rocks are erupted at a sufficiently rapid rate to maintain high temperatures and preclude amphibole crystallization that would otherwise lead to stalling of the mafic magma beneath the surface. Subsequent regrowth of the volcanic edifice returned the magmatic system to conditions less favorable to basaltic magma ascent to the surface and were perhaps associated with increased upper crustal stalling of magmas and the redevelopment of an evolved, andesitic storage system, thus leading to a return to andesitic volcanism at the SHV.

Acknowledgments

We are very grateful to the scientists and crew onboard IODP leg 340, without them this work would not be possible. Stuart Kearns at the University of Bristol is thanked for his assistance with the electron probe analyses. This manuscript was much improved by insightful discussions with Mark Ghiorso, Keith Putirka, Pietro Armienti, and Steve Sparks. Justin Dix is thanked for seeking further financial to support this project. Wall-Palmer acknowledges financial assistance for the stratigraphic dating with grant NE/K002724/1. The AMS radiocarbon dates were provided by the NERC Radiocarbon Facility NRCF010001 (allocation 1721.0513). Cassidy and Watt wish to acknowledge funding from NERC new investigator grant NE/K000403/1. Cassidy also acknowledges an Alexander Von Humboldt fellowship.

The Editor thanks two anonymous reviewers for their assistance in evaluating this paper.

References

Armienti, P., C. Perinelli, and K. D. Putirka (2013), A new model to estimate deep-level magma ascent rates, with applications to Mt. Etna (Sicily, Italy), *J. Petrol.*, *54*(4), 795–813.

Blundy, J., K. V. Cashman, A. Rust, and F. Witham (2010), A case for CO_2-rich arc magmas, *Earth Planet. Sci. Lett.*, *290*(3–4), 289–301.

Boudon, G., B. Villemant, A. Le Friant, M. Paterne, and E. Cortijo (2013), Role of large flank-collapse events on magma evolution of volcanoes. Insights from the Lesser Antilles Arc, *J. Volcanol. Geotherm. Res.*, *263*, 224–237.

Cassidy, M., R. N. Taylor, M. R. Palmer, R. J. Cooper, C. Stenlake, and J. Trofimovs (2012), Tracking the magmatic evolution of island arc volcanism: Insights from a high-precision Pb isotope record of Montserrat, Lesser Antilles, *Geochem. Geophys. Geosyst.*, *13*, Q05003, doi:10.1029/2012GC004064.

Cassidy, M., S. F. L. Watt, M. R. Palmer, J. Trofimovs, W. Symons, S. E. Maclachlan, and A. J. Stinton (2014a), Construction of volcanic records from marine sediment cores: A review and case study (Montserrat, West Indies), *Earth Sci. Rev.*, *138*, 137–155.

Cassidy, M., J. Trofimovs, S. F. L. Watt, M. R. Palmer, R. N. Taylor, T. M. Gernon, P. J. Talling, and A. Le Friant (2014b), Multi-stage collapse events in the South Soufrière Hills, Montserrat, as recorded in marine sediment cores, in *The Eruption of Soufrière Hills Volcano, Montserrat From 2000 to 2010*, Memoirs, edited by G. Wadge, R. Robertson, and B. Voight, Geol. Soc. London, pp. 383–397.

Cassidy, M., M. Edmonds, S. F. L. Watt, M. R. Palmer, and T. Gernon (2015), Arc basalt origin by hybridisation in andesite-dominated arcs, *J. Petrol.*, *56*(2), 325–346.

Davidson, J., S. Turner, H. Handley, C. Macpherson, and A. Dosseto (2007), Amphibole "sponge" in arc crust?, *Geology*, *35*(9), 787–790.

Druitt, T. H., and B. P. Kokelaar (Eds) (2002), *The Eruption of the Soufrière Hills Volcano, Montserrat 1995 to 1999*, Memoirs, Geol. Soc. London.

Erdmann, S., C. Martel, M. Pichavant, and A. Kushnir (2014), Amphibole as an archivist of magmatic crystallization conditions: Problems, potential, and implications for inferring magma storage prior to the paroxysmal 2010 eruption of Mount Merapi, Indonesia, *Contrib. Mineral. Petrol.*, *167*(6), 1016.

Gee, M. A. M., R. N. Taylor, M. F. Thirlwall, and B. J. Murton (1998), Glacioisostacy controls chemical and isotopic characteristics of tholeiites from the Reykjanes peninsula, SW Iceland, *Earth Planet. Sci. Lett.*, *164*(1–2), 1–5.

Gudmundsson, A. (2012), Magma chambers: Formation, local stresses, excess pressures, and compartments, *J. Volcanol. Geotherm. Res.*, *237*, 19–41.

Harford, C. L., M. S. Pringle, R. S. J. Sparks, and S. R. Young (2002), The volcanic evolution of Montserrat using $^{40}Ar/^{39}Ar$ geochronology, in *The Eruption of Soufrière Hills Volcano, Montserrat, From 1995 to 1999*, Memoirs, edited by T. H. Druitt and B. P. Kokelaar, pp. 93–113, Geol. Soc., London.

Hildreth, W. (1981), Gradients in silicic magma chambers: Implications for lithospheric magmatism, *J. Geophys. Res.*, *86*(B11), 10,153–10,192, doi:10.1029/JB086iB11p10153.

Hora, J. M., B. S. Singer, G. Worner, B. L. Beard, B. R. Jicha, and C. M. Johnson (2009), Shallow and deep crustal control on differentiation of calc-alkaline and tholeiitic magma, *Earth Planet. Sci. Lett.*, *285*(1–2), 75–86.

Horwell, C. J., L. P. Brana, R. S. J. Sparks, M. D. Murphy, and V. L. Hards (2001), A geochemical investigation of fragmentation and physical fractionation in pyroclastic flows from the Soufriere Hills volcano, Montserrat, *J. Volcanol. Geotherm. Res.*, *109*(4), 247–262.

Humphreys, M. C. S., M. Edmonds, T. Christopher, and V. Hards (2010), Magma hybridisation and diffusive exchange recorded in heterogeneous glasses from Soufriere Hills Volcano, Montserrat, *Geophys. Res. Lett.*, *37*, L00E06, doi:10.1029/2009GL041926.

Le Friant, A., C. L. Harford, C. Deplus, G. Boudon, R. S. J. Sparks, R. A. Herd, and J. C. Komorowski (2004), Geomorphological evolution of Montserrat (West Indies): Importance of flank collapse and erosional processes, *J. Geol. Soc.*, *161*, 147–160.

Le Friant, A., et al. (2015), Submarine record of volcanic island construction and collapse in the Lesser Antilles Arc: First scientific drilling of submarine volcanic island landslides by IODP Expedition 340, *Geochem. Geophys. Geosyst.*, *16*, 420–442, doi:10.1002/2014GC005652.

Manconi, A., M. A. Longpre, T. R. Walter, V. R. Troll, and T. H. Hansteen (2009), The effects of flank collapses on volcano plumbing systems, *Geology*, *37*(12), 1099–1102.

Manga, M., and E. Brodsky (2006), Seismic triggering of eruptions in the far field: Volcanoes and geysers, *Annu. Rev. Earth Planet. Sci.*, *34*, 263–291.

Metrich, N., and P. J. Wallace (2008), Volatile abundances in basaltic magmas and their degassing paths tracked by melt inclusions, in *Minerals, Inclusions and Volcanic Processes*, *Rev. Mineral. Geochem.*, edited by K. D. Putirka and F. J. Tepley, pp. 363–402, Minerological Society of America.

Pinel, V., and F. Albino (2013), Consequences of volcano sector collapse on magmatic storage zones: Insights from numerical modeling, *J. Volcanol. Geotherm. Res.*, *252*, 29–37.

Pinel, V., and C. Jaupart (2000), The effect of edifice load on magma ascent beneath a volcano, *Philos. Trans. R. Soc. A*, *358*(1770), 1515–1532.

Pinel, V., and C. Jaupart (2005), Some consequences of volcanic edifice destruction for eruption conditions, *J. Volcanol. Geotherm. Res.*, *145*(1–2), 68–80.

Presley, T. K., J. M. Sinton, and M. Pringle (1997), Postshield volcanism and catastrophic mass wasting of the Waianae Volcano, Oahu, Hawaii, *Bull. Volcanol.*, *58*(8), 597–616.

Putirka, K., and C. D. Condit (2003), Cross section of a magma conduit system at the margin of the Colorado Plateau, *Geology*, *31*(8), 701–704.

Putirka, K. D., H. Mikaelian, F. Ryerson, and H. Shaw (2003), New clinopyroxene-liquid thermobarometers for maric, evolved, and volatile-bearing lava compositions, with applications to lavas from Tibet and the Snake River Plain, Idaho, *Am. Mineral.*, *88*(10), 1542–1554.

Ridolfi, F., A. Renzulli, and M. Puerini (2010), Stability and chemical equilibrium of amphibole in calc-alkaline magmas: An overview, new thermobarometric formulations and application to subduction-related volcanoes, *Contrib. Mineral. Petrol.*, *160*(1), 45–66.

Sevilla, W. I., C. J. Ammon, B. Voight, and S. De Angelis (2010), Crustal structure beneath the Montserrat region of the Lesser Antilles island arc, *Geochem. Geophys. Geosyst.*, *11*, Q06013, doi:10.1029/2010GC003048.

Smith, D. J. (2014), Clinopyroxene precursors to amphibole sponge in arc crust, *Nat. Commun.*, *5*, 4329.

Trofimovs, J., et al. (2010), Evidence for carbonate platform failure during rapid sea-level rise; ca 14 000 year old bioclastic flow deposits in the Lesser Antilles, *Sedimentology*, *57*(3), 735–759.

Wadge, G., B. Voight, R. S. J. Sparks, P. D. Cole, S. C. Loughlin, and R. E. A. Robertson (2014), An overview of the eruption of Soufriere Hills Volcano, Montserrat from 2000 to 2010, in *Eruption of Soufriere Hills Volcano, Montserrat From 2000 to 2010*, *Geol. Soc. London, Mem.*, vol. 39, pp. 1–39.

Watt, S. F. L., et al. (2012), Widespread and progressive seafloor-sediment failure following volcanic debris avalanche emplacement: Landslide dynamics and timing offshore Montserrat, Lesser Antilles, *Mar. Geol.*, *323*, 69–94.

Zellmer, G. F., C. J. Hawkesworth, R. S. J. Sparks, L. E. Thomas, C. L. Harford, T. S. Brewer, and S. C. Loughlin (2003), Geochemical evolution of the Soufriere Hills volcano, Montserrat, Lesser Antilles volcanic arc, *J. Petrol.*, *44*(8), 1349–1374.